Applied Catalysis B: Environmental 217 (2017) 125–136

Contents lists available at ScienceDirect

Applied Catalysis B: Environmental

journal homepage: www.elsevier.com/locate/apcatb

Cage-based small-pore catalysts for NH_3-SCR prepared by combining bulky organic structure directing agents with modified zeolites as reagents

Nuria Martín[a], Cecilia Paris[a], Peter N.R. Vennestrøm[b], Joakim R. Thøgersen[b], Manuel Moliner[a,*], Avelino Corma[a,*]

[a] Instituto de Tecnología Química, Universitat Politècnica de València-Consejo Superior de Investigaciones Científicas, Avenida de los Naranjos s/n, 46022 València, Spain
[b] Haldor Topsøe A/S, Haldor Topsøes Allé 1, DK-2800 Lyngby, Denmark

ARTICLE INFO

Article history:
Received 27 March 2017
Received in revised form 23 May 2017
Accepted 27 May 2017
Available online 29 May 2017

Keywords:
Small-pore zeolites
NOx abatement
AFX
Erionite
Organic structure directing agents (OSDAs)

ABSTRACT

It has been possible to efficiently synthesize high-silica ERI and AFX zeolites with nano-sized primary crystallites (30–200 nm). This was achieved by using a dicationic and rigid organic structure directing agent (OSDA) that fits within the large cavities of these zeolites, and the use of FAU zeolites as initial Si- and Al-sources. Cu- and Fe-based ERI and AFX materials were prepared following both post-synthetic cation exchange and direct synthesis methodologies, showing good activity for the selective catalytic reduction (SCR) of nitrogen oxide using ammonia. Accelerated hydrothermal ageing of the zeolites at high temperature (i.e. 750 °C) shows the necessity of removing the alkali cations remaining in the zeolites to obtain stable materials. Furthermore, the catalytic performance of the prepared Cu- and Fe-containing AFX catalysts, both before and after ageing treatment, approaches the catalytic activity of Cu- and Fe-CHA.

1. Introduction

Zeolites are crystalline microporous materials formed by interconnected TO_4 tetrahedra (T = Si, Al...), having uniform pores and cavities with particular sizes and shapes in the molecular dimension range (~3–15 Å) [1,2]. Control of the pore-size openings and cavity dimensions allows the discrimination between organic and inorganic species with geometrical differences of less than 1 Å [3]. These remarkable shape-selective properties together with their high thermal and chemical stabilities, permit their application as ion exchangers, adsorbents or catalysts, among others [4–7].

In the last years, the preparation of small-pore zeolites containing large cavities in their structure has received significant attention [8]. The combination of small pore openings (3-3.5 Å) with large cages offers unique crystalline structures that favor selective diffusion of small molecules [9], while allowing the stabilization of bulky reaction intermediates [10,11] or metallic active sites, from single-atoms to small nanoparticles (less than 1 nm) [12–14]. In particular, small pore zeolites with large cavities have been promoted as efficient catalysts for the methanol-to-olefin (MTO) process [15,16], the selective catalytic reduction (SCR) of NOx typically with ammonia as a reductant [17–19], and the selective oxidation of methane to methanol [20].

Up to now, the catalysts described in the literature that present better activity and hydrothermal stability for the SCR are those based on zeolites with CHA [14,17,19,21] and AEI [22,23] framework topologies (see Fig. 1). These two crystalline frameworks show cavities with intermediate sizes (~8,35 Å, see Fig. 1) that allow hosting and stabilizing of extra-framework metal ions, mainly copper and iron [18], which act as the active centers in NOx reduction. Besides these catalysts, another zeolite containing a cavity with a remarkably larger size, as SSZ-16 (AFX structure, cavity of ~ 8.3 × 13.0 Å, see Fig. 1), was also proposed as an efficient catalyst for the SCR of NOx [24]. Despite the interesting preliminary results achieved with SSZ-16 as a catalyst, very few studies on the use of this topology for SCR are found in the literature [25]. A possible explanation for the low number of reports using SSZ-16 is that the material is only synthesized under limited conditions, resulting in solids with Si/Al molar ratios of 5–6 and relatively large crystal sizes (~ 2–3 μm) [26].

* Corresponding authors.
E-mail addresses: acorma@itq.upv.es (M. Moliner), mmoliner@itq.upv.es (A. Corma).

http://dx.doi.org/10.1016/j.apcatb.2017.05.082
0926-3373/

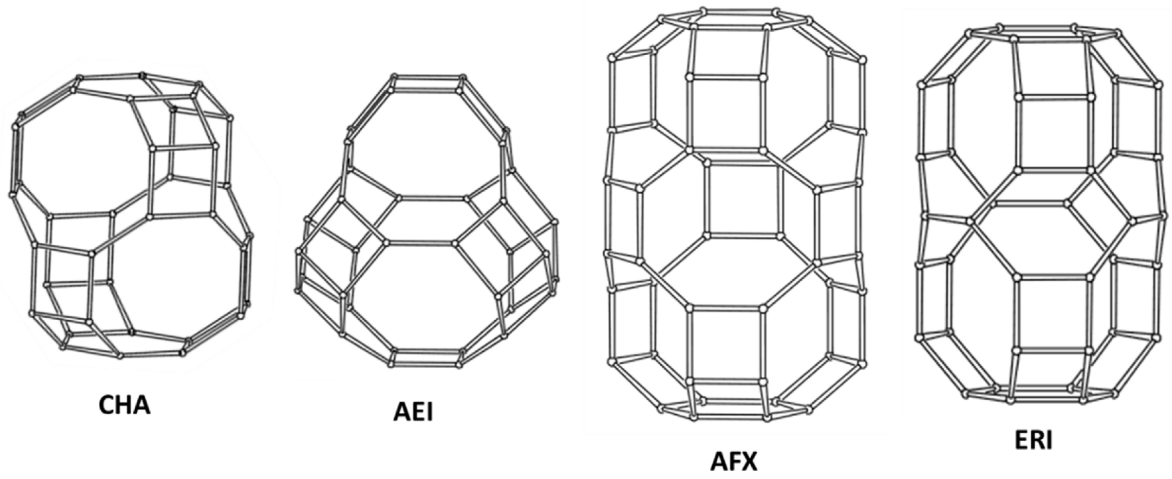

Fig. 1. Cavities present within the structure of different small pore zeolites.

In addition to AFX, another zeolite presenting the combination of small pores with large cavities is erionite (ERI, cavity of ~ 6.3 × 13.0 Å, see Fig. 1) [27]. However, the synthesis of this zeolitic structure in its high-silica form is difficult, and tends to crystallize as an intergrowth with the large pore zeolite offretite (OFF) [28]. Indeed, the ZSM-34 material, which is an intergrowth of ERI and OFF with a Si/Al ratio of ~6, has been reported as a catalyst for the NH_3-SCR reaction [29].

Very recently, the preparation of the AFX and ERI zeolites was optimized by post-synthetic or direct synthesis methods, respectively [30,31]. In one case, the crystal size of the AFX material could be reduced from 3 μm down to almost 100 nm by following a post-milling recrystallization method [30]. In the other case, ERI was directly synthesized as a pure phase by using diverse flexible diquaternary alkylammonium cations as OSDAs, resulting in materials with a Si/Al molar ratio of ~ 5.5, and crystal sizes from 400 nm to 2 μm [31]. To the best of our knowledge, these materials have not yet been tested as catalysts in the selective catalytic reduction of NOx using ammonia.

Despite these advances in the preparation of AFX and ERI, there is still room for optimizing the preparation of these materials. In this sense, the proper selection of the organic molecules that will act as organic structure directing agents (OSDAs) is very important to determine morphological and physical characteristics, such as hydrophobicity, and number of charges introduced by the OSDA molecule [32,33]. In general, it can be said that the selectivity of a particular OSDA towards a specific zeolite increases when the organic molecules present higher size and rigidity [32,33]. At this point, if the preferred OSDAs described for the synthesis of the AFX and ERI are analyzed, it can be seen that both are dicationic large molecules, but present a flexible alkyl chain connecting the two alkyl-ammonium cations [30,31]. The use of flexible OSDAs favors the crystallization of different zeolites depending on the initial synthesis conditions employed, presenting a very low specificity for a particular zeolite [34].

From the potential rigid and bulky molecules that have been described in the literature as efficient OSDAs, polycyclic organic molecules prepared through simple cycloaddition reactions, such as the Diels-Alder reaction, have allowed the synthesis of many new zeolites structures [35]. In general, most of those OSDAs were designed for the synthesis of open structures, preferentially with large pores [36–38]. Indeed, in the past, we have systematically studied several bulky polycyclic OSDAs to attempt the synthesis of high-silica, and even pure silica or metallosilicate, large-pore zeolites under broad synthesis conditions using high-throughput systems, and selecting in all cases Si/Al ratios higher than 15 [38,39]. However, if one analyses carefully the catalysts reported in the literature for the SCR, it is observed that the most active and stable materials are those presenting small pores, large cavities and relatively low Si/Al ratios (preferentially between 5 and 15). Thus, it could be envisaged that bulky and rigid OSDAs, such as those proposed in Fig. 2, could be good candidates to stabilize the formation of the large cavities of some small-pore zeolites if they were tested under more appropriate synthesis conditions, such as for instance lower Si/Al molar ratios.

Moreover, it is well-known that the initial Si and Al sources selected to overcome the zeolite synthesis may influence the nucleation and crystallization processes involved during the hydrothermal preparation [40]. Their different dissolution-precipitation mechanisms could affect the crystallization, allowing the formation of different zeolites depending if amorphous or crystalline initial sources are used [40]. In the last years, different crystalline zeolites, particularly high-silica FAU zeolites, have been intensively employed as initial silicon and aluminum sources [23,41–44]. Some of the reported advantages of using these precrystalline materials as precursors are the presence of the required heteroatoms (i.e. Al) in tetrahedral coordination, which would favor their incorporation in the final product [45,46], and also the presence of some secondary building units (SBUs), which would favor formation of zeolites also containing these SBUs [44,47]. Interestingly, the faster nucleation observed using some crystalline zeolites as initial precursors has resulted in the formation of nanocrystalline zeolites [16,48–50].

Herein, two bulky and rigid dicationic organic molecules have been studied as OSDAs for the synthesis of small-pore zeolites with large cavities. In this sense, the two organic molecules have been prepared through simple cycloaddition reactions, presenting different size and shape (see OSDA-1 and OSDA-2 in Fig. 2). The synthesis of zeolites has been attempted under a set of broad conditions, including the use of different Si and Al sources and alkali cations. The OSDA-2 cation allows the formation of two different small-pore zeolites, ERI and AFX, both presenting large cavities within their structures (see Fig. 1), when using FAU zeolites as initial Si- and Al-sources. The syntheses of ERI and AFX requires the presence of K^+ and Na^+ cations, respectively, resulting in materials with smaller crystal sizes than those previously reported in the literature. These materials have been evaluated in the NH_3-SCR reaction, after introducing copper and iron by post-synthetic cation-exchange or direct synthesis procedures. Cu- and Fe-containing ERI and AFX solids show high activity in the reaction

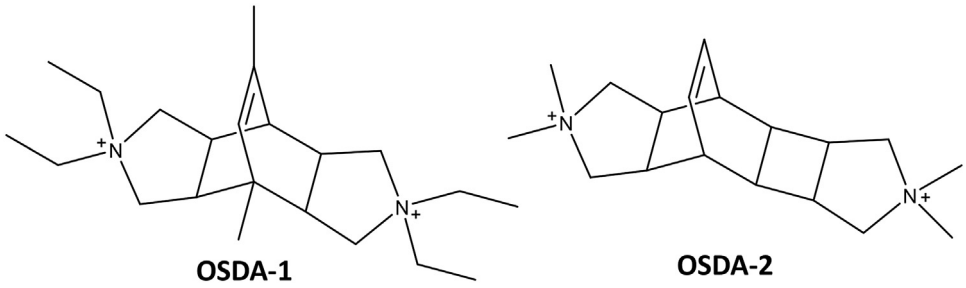

Fig. 2. Organic structure directing agents selected to attempt the synthesis of small pore zeolites containing large cavities.

as well as high hydrothermal stability, especially when the alkali cations are selectively removed from the final catalysts.

2. Experimental

2.1. Synthesis of the OSDAs

2.1.1. OSDA-1

161 mmol of 4,6-dimethyl-α-pyrone and 322 mmol of maleic anhydride were dissolved in 500 mL of toluene, and the resultant solution refluxed during 5 days. After cooling, the precipitate was filtered and washed with hexane to give the corresponding bicyclodianhydride. Then, 140 mmol of the bicyclodianhydride product was dissolved in 400 mL of an ethylamine solution (70% in H_2O), being maintained under reflux for 4 days. Afterwards, the solvent was removed using a rotary evaporator, resulting in the diimine product.

At this point, 49 mmol of the diimine was slowly added to a suspension of $LiAlH_4$ (244 mmol) in anhydrous THF (300 mL) at 0 °C under N_2 atmosphere, and the mixture was refluxed for 5 h and stirred at room temperature overnight. The reaction was quenched by adding 10 mL of H_2O, 10 mL of a solution of NaOH (15% in water) and 10 mL of H_2O, remaining under stirring at room temperature for 30 min. Afterwards, the solution was filtered and extracted with dichloromethane. The organic extracts were washed with brine, dried and concentrated to dryness, providing the corresponding diamine product.

Finally, 52 mmol of the diamine was dissolved in 70 mL of methanol, and 642 mmol of CH_3I was slowly added. The mixture was stirred at room temperature for 3 days. Then, the final organic dication was concentrated under vacuum and precipitated by addition of diethyl ether. The resultant iodide salt was exchanged to the hydroxide using a commercially available hydroxide ion exchange resin (Dowex SBR).

2.1.2. OSDA-2

108 mmol of N-methylmaleimide was added in a mixture of benzene (300 mL), acetophenone (30 mL), and acetone (84 mL). The solution was introduced in Pyrex tubes, flowing N_2 for 15 min. Afterwards, a photochemical reaction was carried out by irradiation using a high pressure Hg lamp ($200 < \lambda < 90$ nm) for 48 h under stirring. The resulting precipitate was filtered under vacuum providing the desired diimide.

At this point, 49 mmol of the diimine was slowly added to a suspension of $LiAlH_4$ (244 mmol) in anhydrous THF (300 mL) at 0 °C under N_2 atmosphere, and the mixture was refluxed for 5 h and stirred at room temperature overnight. The reaction was quenched by adding 10 mL of H_2O, 10 mL of a solution of NaOH (15% in water) and 10 mL of H_2O, remaining under stirring at room temperature for 30 min. After 30 min stirring at room temperature the solution was filtered, partially concentrated in the rotary evaporator and then extracted with dichloromethane. The organic extracts were washed with brine, dried and concentrated to dryness, providing the corresponding diamine product.

Finally, 34 mmol of the diamine was dissolved in 85 mL of methanol, and 1 mol of CH_3I was slowly added. The mixture was stirred at room temperature for 7 days. Then, the final organic dication was concentrated under vacuum and precipitated by addition of diethyl ether. The resultant iodide salt was exchanged to the hydroxide using a commercially available hydroxide ion exchange resin (Dowex SBR).

Table 1
Synthesis variables explored for each OSDA molecule.

Variable	Range
Si/Al	6, 10, 15
OSDA/Si	0.2, 0.4
MOH/Si (M = Na, K)	0, 0.2
H_2O/Si	5, 15
T (°C)	135, 175
Si sources	Ludox, Aerosil, FAU (Si/Al = 6, 11, 25)
Al source	$Al(OH)_3$
Total experiments	**72**

2.2. Synthesis of zeolites using OSDA-1 and OSDA-2

The hydrothermal synthesis conditions applied are summarized in Table 1. In general, the following procedure was employed: the required content of the aqueous solutions of the OSDAs in their hydroxide form was mixed with the required content of 20%wt aqueous solutions of the alkali hydroxides (NaOH or KOH, Sigma-Aldrich). Afterwards, the required amounts of the silicon and/or aluminum sources [Ludox AS-40 (Sigma-Aldrich, 40%wt), fumed silica (Aerosil), FAU zeolites with various Si/Al ratios (CBV712 with Si/Al ∼6, CBV720 with Si/Al ∼11, and CBV760 with Si/Al ∼26, all from PQ-Industries), and $Al(OH)_3$ (Sigma-Aldrich, 58%)] were added to the previous solution, maintaining the synthesis mixture under stirring for the required time to evaporate excess of water until achieving the desired gel concentration. The resultant gels were charged into stainless steel autoclaves with Teflon liners, and the crystallizations were conducted at the required temperature (135 or 175 °C) for 10 days under static conditions. The solids were filtered, washed with water, and dried at 100 °C. The calcination of the solid samples to remove the organic molecules occluded within the crystals was performed in air at 580 °C for 6 h.

2.2.1. Cu-exchange procedure

The Cu ion exchange of the calcined zeolites was carried out by introducing 0.22 g of zeolite within 22 mL of an aqueous solution of $Cu(CH_3CO_2)_2$ [15.8 mg of $Cu(CH_3CO_2)_2$ dissolved in 22 mL of water], maintaining a solid/liquid ratio of 10 g/L at room temperature for 10 h. Finally, the sample was filtered and washed with distilled water, and calcined at 500 °C for 4 h.

The previous elimination of the alkali cations from the calcined zeolites was carried out by exchange with an aqueous solution of

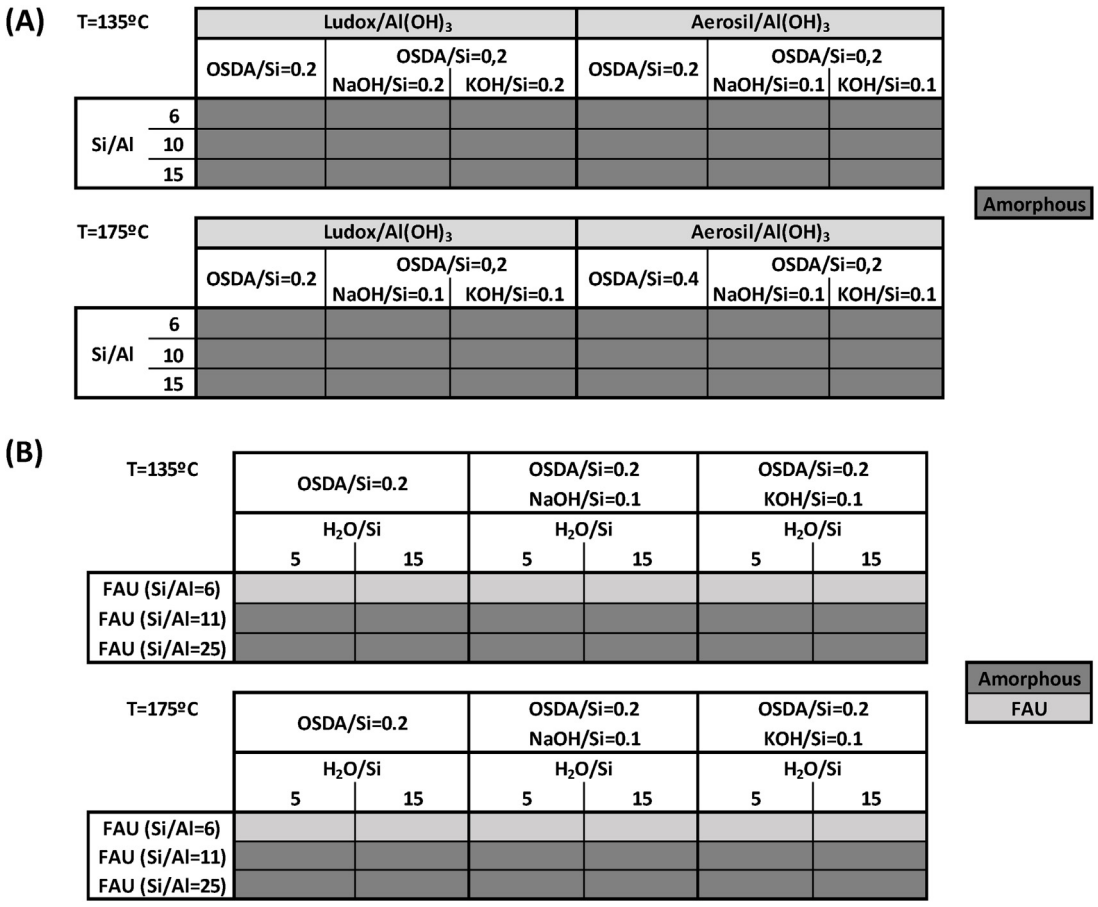

Fig. 3. Phase diagrams achieved when using OSDA-1 with Ludox/Aerosil and $Al(OH)_3$ as silicon and aluminum sources (A) or commercially available FAU zeolites (B).

NH_4Cl. For this purpose, 0.5 g of sample was exchanged with 5 mL of a 1 M aqueous solution of NH_4Cl, maintaining a solid/liquid ratio of 10 g/L at room temperature for 10 h. Afterwards, the samples were exchanged with an aqueous solution of $Cu(CH_3CO_2)_2$ as described above.

2.2.2. One-pot synthesis procedure to prepare Fe-containing zeolites

For the direct synthesis of the iron-containing zeolites, the required amount of a 20%wt aqueous solution of iron (III) nitrate [$Fe(NO_3)_3$, Sigma Aldrich, 98%] was added together with the silicon and aluminum sources, according to the general synthesis methodology described above. The final gel compositions for the Fe-ERI and Fe-AFX were the following:

Fe-ERI : Si/0.166Al/0.01Fe/0.1KOH/0.2OSDA-2/5 H_2O

Fe-AFX : Si/0.166Al/0.01Fe/0.1NaOH/0.2OSDA-2/15 H_2O

In these two syntheses, the source of silicon and aluminum was the commercially available FAU zeolite with a Si/Al ratio of 6 (CBV712, PQ-industries), and the crystallization conditions were 175 °C for 7 days. The solids were filtered, washed with water, and dried at 100 °C. The calcination of the solid samples to remove the organic molecules occluded within the crystals was performed in air at 580 °C for 4 h.

The alkali-containing Fe-ERI and Fe-AFX materials were mixed with a 1 M aqueous solution of ammonium chloride (100 mg solid/1 mL liquid), and the mixture was maintained under stirring at 80 °C for 5 h. The solid product was filtered, washed with abundant water, and dried at 100 °C. Finally, the solid was calcined in air at 500 °C for 4 h.

2.3. Characterization

Powder X-ray diffraction (PXRD) measurements were performed with a multisample Philips X'Pert diffractometer equipped with a graphite monochromator, operating at 40 kV and 35 mA, and using Cu Kα radiation (λ = 0,1542 nm). The chemical analyses were carried out in a Varian 715-ES ICP-Optical Emission spectrometer, after solid dissolution in HNO_3/HCl/HF aqueous solution. The organic content of as-made materials was determined by elemental analysis performed with a SCHN FISONS elemental analyzer. UV–vis spectra were obtained with a Perkin–Elmer (Lambda 19) spectrometer equipped with an integrating sphere with $BaSO_4$ as reference. The morphology of the samples was studied by scanning electron microscopy (SEM) using a JEOL JSM-6300 microscope.

The NMR spectra were recorded at room temperature with a Bruker AV 400 spectrometer. ^{29}Si MAS NMR were recorded with a spinning rate of 5 kHz at 79.459 MHz with a 55° pulse length of 3.5 μs and repetition time of 180s. ^{27}Al MAS NMR spectra were recorded at 104.2 MHz with a spinning rate of 10 kHz and 9° pulse length of 0.5 μs and repetition time of 1 s. ^{29}Si and ^{27}Al chemical shifts were referred to tetramethylsilane and $Al^{3+}(H_2O)_6$, respectively.

Textural properties were determined by N_2 adsorption isotherms measured at 77 K with a Micromeritics ASAP 2020.

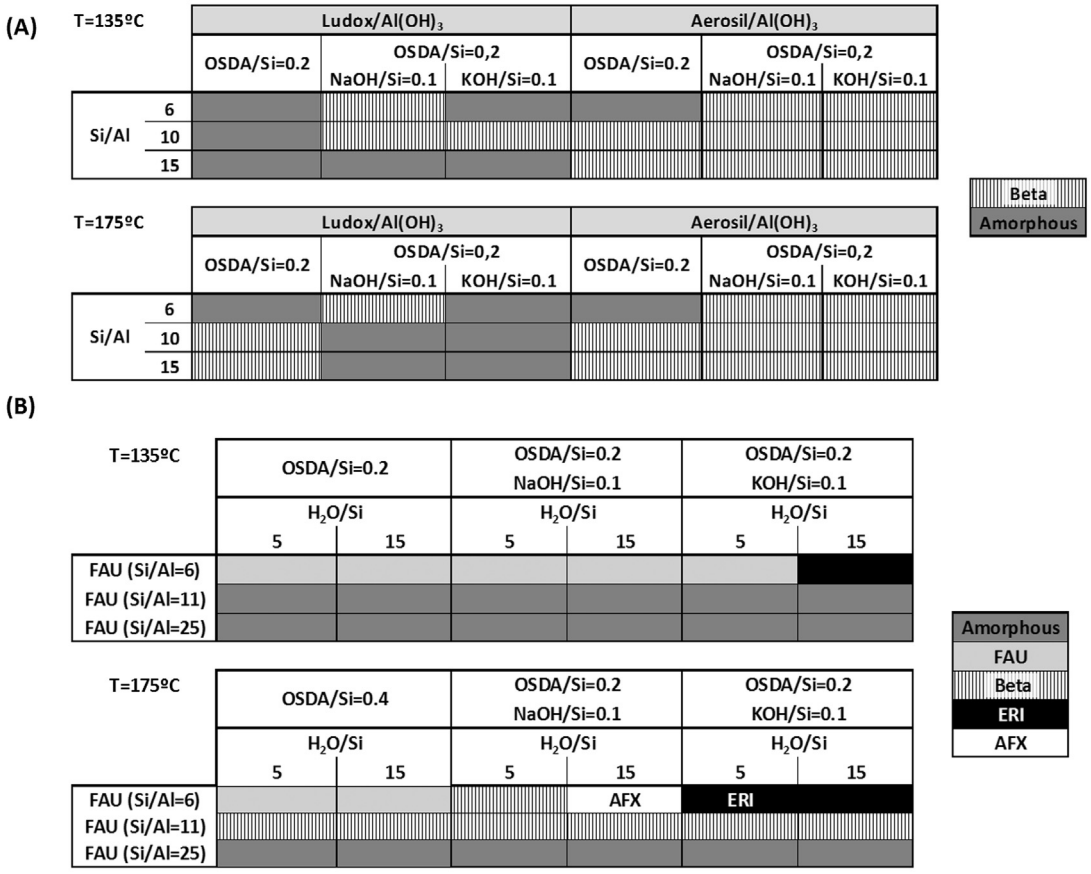

Fig. 4. Phase diagrams achieved when using OSDA-2 with Ludox/Aerosil and $Al(OH)_3$ as silicon and aluminum sources (A) or commercially available FAU zeolites (B).

Table 2
Elemental analyses of as-prepared materials.

Sample	%wt N	%wt C	C/N	OSDA-2/supercavity
ERI	2.02	15.32	8.8	1.0
AFX	1.84	14.51	9.2	1.1

2.4. Accelerated hydrothermal ageing treatment

A severe accelerated ageing of the metal-containing molecular sieves was performed by steaming the solids in a muffle furnace in 100% H_2O for 13 h at 750 °C (water flow ~2. 2 mL/min).

2.5. Catalytic testing: selective catalytic reduction of NO using ammonia

The catalytic activity was evaluated for the catalytic reduction of NOx with NH_3 in a fixed bed, quartz tubular reactor of 1.2 cm of diameter and 20 cm of length. The catalysts were tested using 40 mg with a sieve fraction of 0.25-0.42 mm. The catalysts were introduced in the reactor and heated up to 550 °C in a 300 mL/min flow of nitrogen and maintained at this temperature for one hour. Afterwards, the feed was admitted over the catalyst while maintaining a flow of 300 mL/min. The feed composition for the catalytic tests performed over the Cu-containing catalysts was 500 ppm NO, 530 ppm NH_3, 7% O_2 and 5% H_2O; while the feed composition for the catalytic tests performed over the Fe-containing catalysts was 50 ppm NO, 60 ppm NH_3, 10% O_2 and 10% H_2O. The reaction temperature was decreased stepwise between 550 and 170 °C. The conversion of NO was measured under steady state conversion at each temperature using a chemiluminiscence detector (Thermo 62C).

3. Results

3.1. Synthesis of zeolites

The synthesis of zeolites using the OSDA molecules shown in Fig. 2 was attempted under the conditions summarized in Table 1. The tested conditions represent a broad set of phase-space, including the use of different Si- and Al-sources (Ludox AS-40, aerosil and pre-crystalized FAU zeolites with different Si/Al ratios), different alkali cations (sodium and potassium), different crystallization temperatures (135 and 175 °C), and different molar ratios for several of the components: Si/Al [6,10,15]; OSDA/Si [0.2,0.4]; alkaline/Si [0,0.2], and H_2O/Si [5,15]. With these variables, 72 syntheses were carried out for each OSDA (see Table 1).

The phase diagrams achieved when using OSDA-1 as template are shown in Fig. 3. As seen, the OSDA-1 molecule does not allow crystallizing of any zeolitic phase within the tested time frame, even when using different commercially available FAU zeolites as initial precursors in the synthesis media (see Fig. 3). The presence of methyl groups in axial positions within the OSDA-1 molecule could be one of the reasons for the low templating effects of this organic molecule under the studied conditions, precluding the stabilization of the large cavities, and consequently, the crystallization of any cavity-based small-pore zeolite.

The OSDA-2 molecule shows a similar length compared to OSDA-1, but it does not contain alkyl groups in axial positions (see OSDA-2 in Fig. 2). The OSDA-2 was tested under similar conditions as OSDA (see Table 1). The use of Ludox and Aerosil as Si-sources allowed the crystallization of large-pore Beta zeolite under different synthesis conditions (see Fig. 4A). This result is not unexpected since OSDA-2 has indeed been reported as template for the synthe-

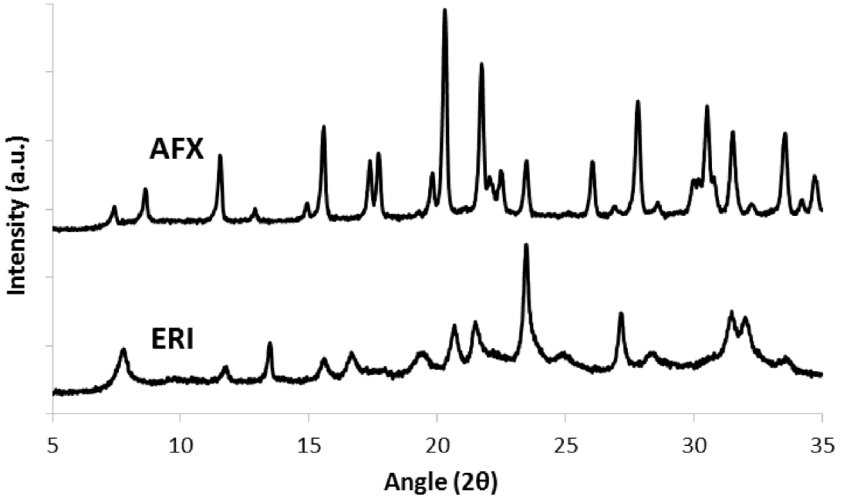

Fig. 5. PXRD patterns of the as-prepared ERI and AFX samples.

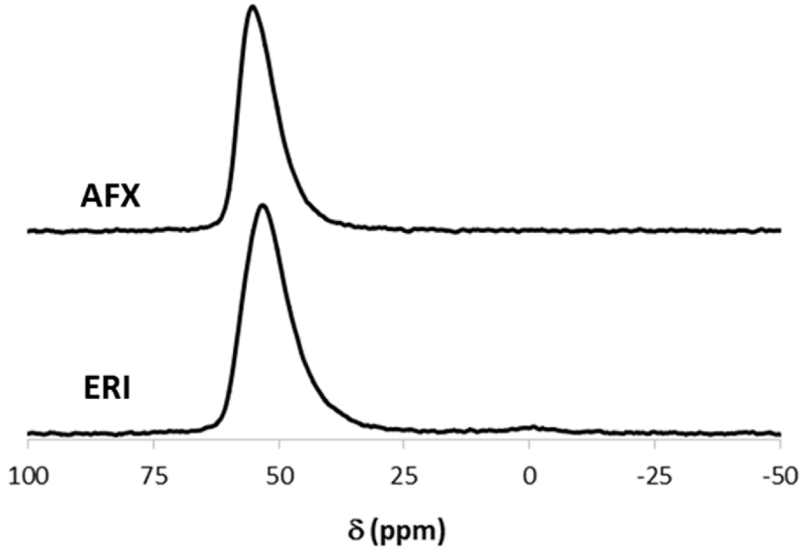

Fig. 6. ^{27}Al MAS NMR spectra of the as-prepared ERI and AFX samples.

sis of the polymorph C of the Beta zeolite (BEC framework topology) [39]. However, the combination of FAU with a Si/Al ratio of ~6 as a Si- and Al-source and OSDA-2 results in the crystallization of two different zeolites, namely, erionite (ERI) and SSZ-16 (AFX), depending on the additional presence of potassium or sodium cations in the synthesis media, respectively (see ERI and AFX in Fig. 4B). It is important to note that both ERI and AFX structures present a common secondary building unit (SBU) with the initial FAU precursor, which is the double-6-ring (D6R).

PXRD patterns of the as-prepared ERI and AFX materials reveal the crystallization of these structures as pure phases (see Fig. 5). As it has been stated above, both crystalline structures show the presence of large cavities with similar length (~13.0 Å, see Fig. 1), suggesting that the bulky and rigid OSDA-2 presents the adequate shape and size (11.9 × 4.9 Å) to properly fit and stabilize these cavities. Elemental analyses on the as-prepared ERI and AFX materials were carried out to quantify the amount of the organic molecules entrapped within the crystals of these materials, and to evaluate their stability during the zeolite crystallizations. As it can be seen in Table 2, both as-prepared materials show similar organic contents, and the analyzed C/N molar ratios were close to 9, which corresponds to the theoretical C/N molar ratio of the intact OSDA-2 molecule. Furthermore, the amount of OSDA-2 in each sample indicate that all super-cavities present in both materials are filled by one OSDA-2 molecule (1.0 and 1.1 OSDA-2/supercavity for ERI and AFX, respectively). These results demonstrate not only the excellent directing effects of the OSDA-2 molecules toward the large cavities present in ERI and AFX structures, but also the excellent stability of these organic molecules under the severe reaction conditions required during the hydrothermal syntheses (high pHs and temperatures).

Interestingly, the solid yields observed after the hydrothermal crystallization of both materials are very good (above 85%), indicating that most of the silicon and aluminum species introduced in the initial gels have been incorporated in the final zeolitic crystals. Indeed, the measured Si/Al molar ratios of the ERI and AFX materials are almost identical (~5.2-5.3, see Table 3), and similar to the Si/Al molar ratio of the initial FAU zeolitic precursor, confirming the incorporation of the Si and Al species in the crystals of both final solids.

To evaluate the successful incorporation of the aluminum species in framework positions, the two as-prepared ERI and AFX materials were characterized by ^{27}Al MAS NMR spectroscopy. As seen in Fig. 6, only a single band centered at ~55 ppm for both sam-

Table 3
ICP analyses of synthesized materials.

Sample	Si/Al	Na/Al	K/Al	%wt Cu	%wt Fe
ERI	5.2	–	0.55	–	–
AFX	5.3	0.35	–	–	–
Cu-ERI_exc1	5.1	–	0.41	2.2	–
Cu-AFX_exc1	5.3	0.19	–	3.1	–
Cu-ERI_exc2	5.2	–	0.15	2.8	–
Cu-AFX_exc2	5.2	0.00	–	3.0	–
Fe-ERI	5.1	–	0.44	–	1.07
Fe-AFX	5.3	0.40	–	–	1.01
Fe-ERI_exc	5.2	–	0.21	–	1.03
Fe-AFX_exc	5.2	0.01	–	–	0.95

Table 4
Textural properties of calcined ERI and AFX materials.

Sample	BET surface area (m^2/g)	Micropore area (m^2/g)	External surface area (m^2/g)	Micropore volume (cm^3/g)
ERI	598	448	150	0.22
Cu-ERI_exc2_HT750	312	196	116	0.09
AFX	590	570	20	0.28

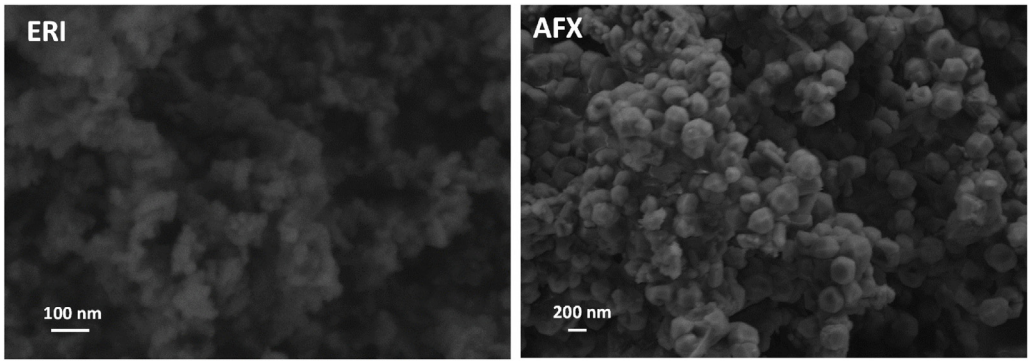

Fig. 7. SEM images of the as-prepared ERI and AFX samples.

ples are observed, which has been assigned to aluminum atoms in tetrahedral coordination, indicating the selective incorporation of all aluminum into the zeolite frameworks of ERI and AFX.

The two AFX and ERI samples were also characterized by FE-SEM microscopy to analyze the crystal size of the obtained materials. ERI and AFX samples show a homogeneous crystal size distribution, with small crystals in both cases (~30 and ~200 nm, respectively, see Fig. 7). Such small crystal sizes indicate that organic-inorganic interactions are affected during the early stages of crystallization and indicate that especially nucleation is affected.

Each of the samples were calcined in air at 580 °C for 6 h to remove the organic molecules occluded in their cavities. N_2 adsorption was then used to evaluate their microporous (see isotherms in Fig. 8). As seen in Table 4, ERI and AFX materials show high micropore areas (448 and 570 m^2/g, respectively) and micropore volumes (0.22 and 0.28 cm^3/g, respectively), as expected. Regarding the external surface areas, ERI presents a higher value than AFX due to the substantially lower crystal size observed in the former material (see Table 4).

3.2. Catalytic performance in NH_3-SCR of NO

3.2.1. Copper containing AFX and ERI

The ability to prepare AFX and ERI small pore zeolites with high crystallinity, porosity and aluminum in framework positions allows for simple aqueous exchange of copper ions in order to evaluate the catalytic performance in the selective catalytic reduction of NO using NH_3.

Both calcined ERI and AFX materials were exchanged with an aqueous solution of copper acetate at room temperature to achieve the corresponding copper-containing materials (see more details in the experimental section). The amount of copper in the final solids after the exchange procedures is ~2-3%wt (see Cu-ERI_exc1 and Cu_AFX_exc1 in Table 3), which is usually considered an optimum for the NH_3-SCR reaction [19,21,22,24]. As expected, the amount of alkali cations after Cu-exchange is lowered for both solids, but some alkali cations still remain within the final solids (K/Al ~0.4 and Na/Al ~0.2 for Cu-ERI_exc1 and Cu-AFX_exc1, respectively, see Table 3).

The Cu-exchanged ERI and AFX materials were tested in their fresh state, observing in both cases high conversion of NO (~80-90%) for most of the reaction temperatures tested (see Cu-ERI_exc1 and Cu-AFX_exc1 in Fig. 9A and B, respectively) and with comparable conversion profiles to what we usually observe for Cu exchanged CHA materials. However, when the Cu-AFX_exc1 and Cu-ERI_exc1 were aged under severe conditions to evaluate their hydrothermal stability (steaming at 750 °C for 13 h), their crystalline structure collapsed (see PXRD patterns of Cu-ERI_exc1_HT750 and Cu-AFX_exc1_HT750 in Fig. 10).

The presence of alkali and alkaline-earth metal cations in other small-pore zeolites has earlier been reported to affect catalytic activity as well as the hydrothermal stability [21,51]. Taking that into account, we decided to prepare materials where the alkali content is minimized before copper exchange. In this sense, the initially calcined K-containing ERI and Na-containing AFX materials were first exchanged with ammonium chloride to selectively remove most of these alkali cations, and later, the desired content of copper

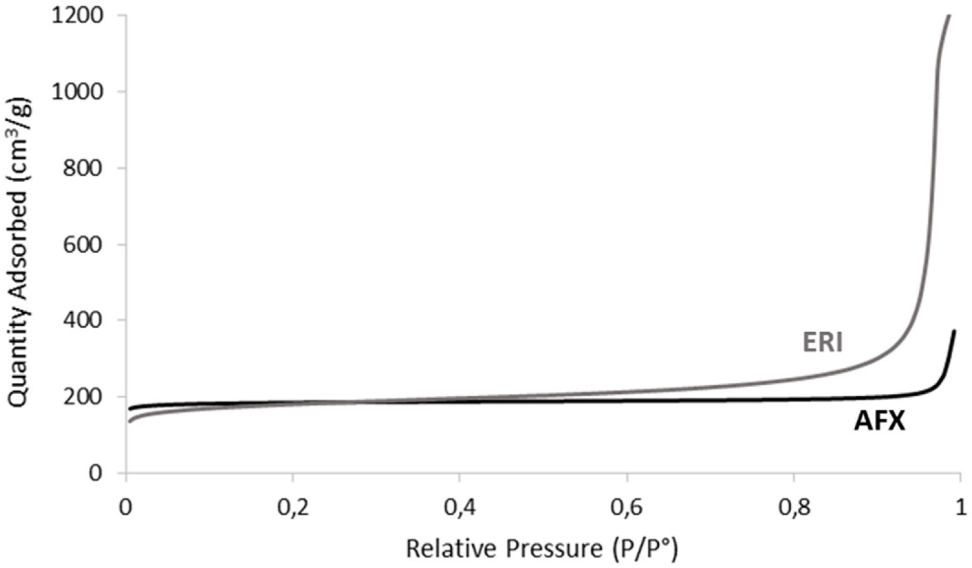

Fig. 8. N_2 adsorption isotherms for the calcined ERI and AFX zeolites.

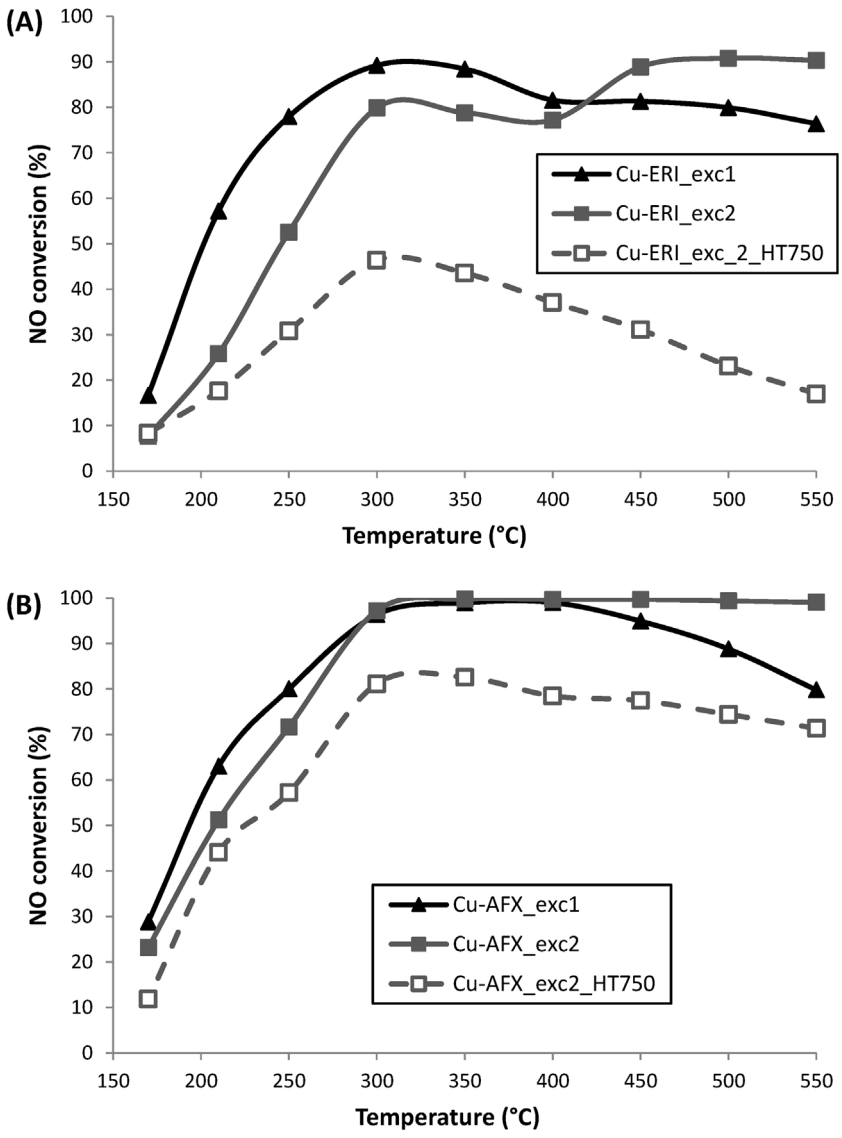

Fig. 9. Measured NO conversion over copper-containing ERI-related (A) and AFX-related (B) materials in the NH_3-SCR reaction.

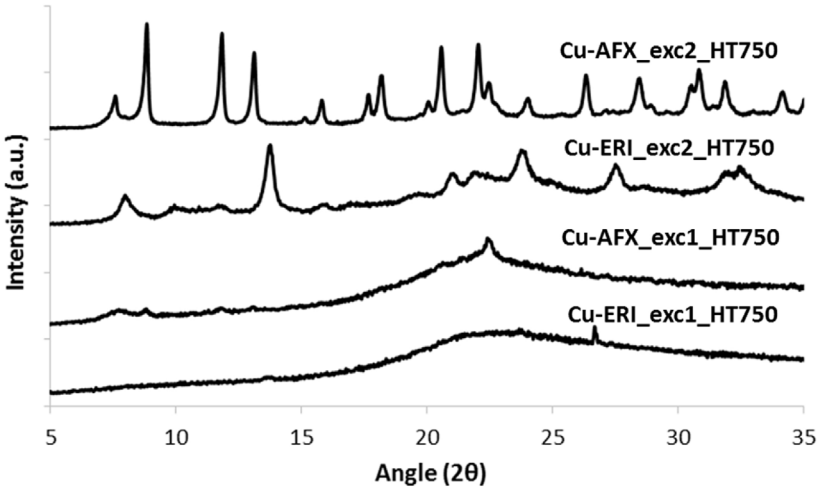

Fig. 10. PXRD patterns of the Cu-exchanged ERI and AFX samples after steaming at 750 °C for 13 h.

has been introduced through a second cation-exchange procedure with copper acetate (see experimental section). After this two-step exchange procedure, the Cu-containing ERI material contained ~2.8%wt of Cu, as well as some potassium cations in the final solid (K/Al ~0.15, see Cu-ERI_exc2 in Table 3). Nevertheless, this potassium content is remarkably lower than in the Cu-containing ERI sample where the copper was directly exchanged (K/Al ~0.15 and 0.41 for Cu-ERI_exc2 and Cu-ERI_exc1, respectively, see Table 3). In contrast, the Cu-containing AFX material contains ~3.0%wt of Cu, and this solid is essentially free of alkali cations after the two-step exchange procedure (Na/Al ~0.00, see Cu-AFX_exc2 in Table 3).

The two-step exchanged Cu-ERI and Cu-AFX materials show in general improved catalytic behavior when compared to their corresponding alkali-containing forms, particularly under high reaction temperatures (above 350 °C, see Cu-ERI_exc2 and Cu-AFX_exc2 in Fig. 9A and B, respectively). Nevertheless, it is important to note that the sample that is essentially free of alkali cations, Cu-AFX_exc2, performs better than the Cu-ERI_exc2, which still contains some potassium cations after the two-step cation exchange procedure (see Fig. 9A and B). This fact is in agreement with recent results describing the negative influence of the alkali and alkaline-earth cations within the Cu-containing small pore zeolites when used as catalysts for the SCR of NOx [51].

The two-step exchanged Cu-ERI and Cu-AFX materials mostly maintain their crystalline structure after severe hydrothermal treatment (100% steam at 750 °C for 13 h) as seen by PXRD after the treatment (Cu-ERI_exc2_HT750 and Cu-AFX_exc2_HT750 in Fig. 10). Nevertheless, it should be noted that the catalytic behavior of the aged materials for the NH_3-SCR is different. On the one hand, the aged Cu-ERI_exc2 sample shows decreased NO conversions in the entire temperature range (below 40%, see Cu-ERI_exc2_HT750 in Fig. 9A). In order to evaluate if a partial collapse of the crystalline structure of the Cu-containing ERI after the ageing treatment would explain the loss of catalytic activity, the aged Cu-ERI_exc2_HT750 sample has been characterized by ^{29}Si MAS NMR spectroscopy and N_2 adsorption. As seen in Fig. 11, the ^{29}Si MAS NMR spectrum of the Cu-ERI_exc2_HT750 shows small variations in the intensity of the signals associated to the crystallographic positions of silicon when compared to its fresh counterpart, suggesting that the crystalline structure of the ERI zeolite could be suffering, at least, a partial collapse during the severe ageing treatment. This point is confirmed by the characterization of the aged Cu-containing ERI zeolite by N_2 adsorption, as revealed by the decrease of the BET surface area and micropore volume (see Cu-ERI_exc2_HT750 in Table 4). On the other hand, the aged and essentially alkali-free Cu-AFX_exc2 gives NO conversion values of ~80% for reaction temperatures comprised between 300 and 550 °C (see Cu-AFX_exc2_HT750 in Fig. 9B). These catalytic results are lower than those described for optimized and well-established industrial catalysts in the literature, as for instance Cu-CHA, when tested and aged following similar severe conditions [52]. It is important to remark that the optimized industrial Cu-CHA catalysts has higher Si/Al molar ratios (preferentially above 9) than the achieved here for the AFX material (~5.3). Therefore, it could be expected that if the Si/Al molar ratio within the AFX-based catalysts could be increased, their hydrothermal stability could mimic, or even surpass, the hydrothermal stability of the well-established industrial CHA-based SCR catalysts.

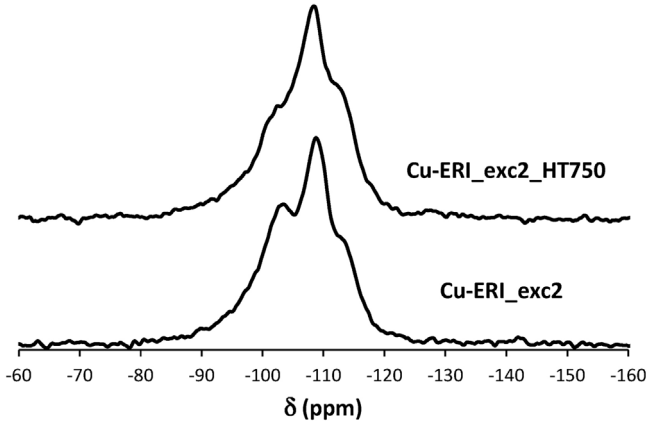

Fig. 11. ^{29}Si MAS NMR spectra of Cu-ERI_exc2 before and after the steaming treatment.

Though there is not a clear explanation for the adverse effects of the alkali and alkaline-earth cations within the Cu-containing small pore zeolites, it could be envisioned that one possible reason could be the competitive charge balance between extra-framework sodium and copper species. The results achieved for the Cu-containing ERI and AFX highlight the importance of, at least in some cases, to properly remove alkali cations from Cu-containing zeolite-based catalysts not only to improve their hydrothermal stability but also their catalytic activity for SCR of NOx applications.

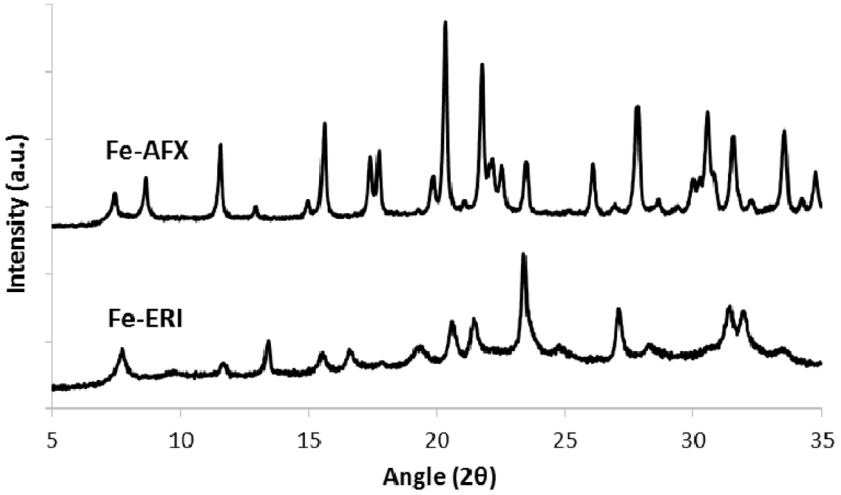

Fig. 12. PXRD patterns of the as-prepared one-pot synthesized Fe-containing ERI and AFX samples.

3.2.2. Iron-containing zeolites

Besides the introduction of copper species within zeolite structures to create efficient and stable catalysts for NH_3-SCR, the preparation of iron-containing small-pore zeolites has also being proposed in the last years [53,54]. This could be mainly attributed to their better NH_3-SCR performance at high temperatures (above 400 °C) compared to the copper containing analogs [55].

Taking the above into account, we present here the direct syntheses of iron-containing ERI and AFX zeolites under the optimized conditions shown in Fig. 4B. For this purpose, the required amount of an iron salt was added to the synthesis gels of ERI and AFX to get a final Si/Fe of ~100 (see experimental conditions). The resultant solids after the hydrothermal crystallization processes show the characteristic PXRD patterns of the crystalline structures of ERI and AFX (see Fig. 12).

The UV–vis spectra of the as-prepared Fe-ERI and Fe-AFX zeolites show the presence of two main bands centered at 215 and 240 nm, which have been assigned to iron species in tetrahedral coordination within the zeolite frameworks (see Fe-ERI_a.p. and Fe-AFX_a.p. in Fig. 13) [56,57]. In contrast, when these Fe-ERI and Fe-AFX zeolites were calcined in air at 580 °C, a new band appears at ~275 nm, which has been assigned to the presence of cationic

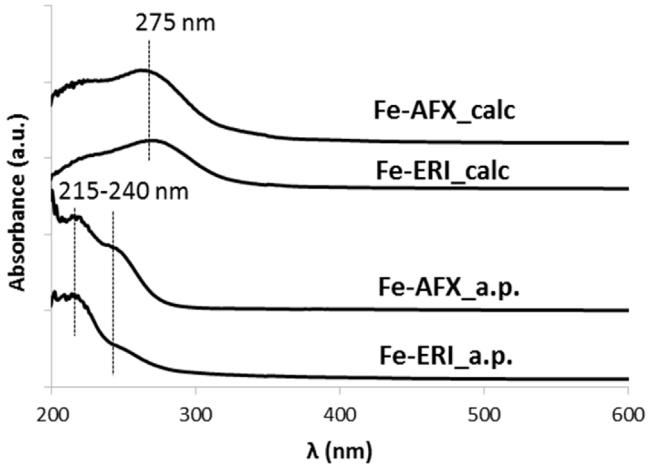

Fig. 13. UV–vis spectra of the as-prepared and calcined one-pot synthesized Fe-containing ERI and AFX samples.

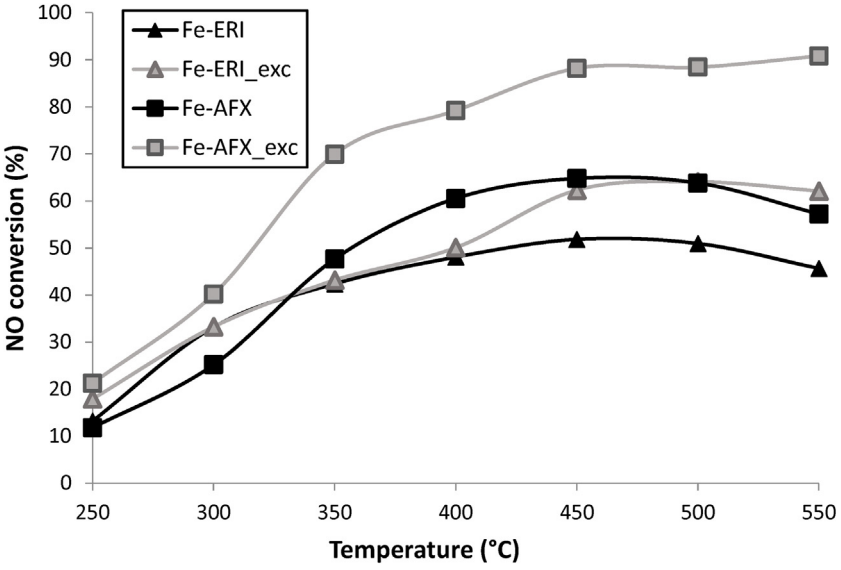

Fig. 14. Measured NO conversion over iron-containing ERI and AFX materials in the NH_3-SCR reaction.

iron species in extra-framework positions (see Fe-ERI_calc and Fe-AFX_calc in Fig. 13).

ICP analysis of the Fe-ERI and Fe-AFX zeolites reveals similar Si/Al ratios and iron contents for both materials (Si/Al ~5.1-5.3 and %wt Fe ~1.0-1.1, see Table 3). In addition, these solids also present a high content of alkali cations (Alkali/Al ~0.4, see Fe-ERI and Fe-AFX in Table 3). The calcined Fe-ERI and Fe-AFX catalysts were first tested in the NH_3-SCR reaction under conditions relevant for this type of materials (see experimental section). As seen, both Fe-based catalysts show intermediate NO conversion values of 40 and 60% at high reaction temperatures for Fe-ERI and Fe-AFX, respectively (see Fig. 14). As it was observed above with the copper-containing zeolites, the presence of alkali metal cations mostly preclude the catalytic activity of the iron-based zeolite catalysts for the SCR of NOx [54]. Thus, a cation exchange procedure with ammonium chloride was also performed for the two iron-containing zeolites to remove potassium or sodium cations (see experimental section). The resultant ammonium-exchanged Fe-ERI and Fe-AFX zeolite materials present similar Fe amount than the as-prepared solids (~1.0%wt Fe, see FeERI_exc and Fe-AFX_exc in Table 3), while the alkali metal contents are substantially reduced (K/Al ~0.21 and Na/Al ~0.01 for FeERI_exc and Fe-AFX_exc, respectively, see Table 3). Afterwards the two ammonium-exchanged materials were again tested in the NH_3-SCR reaction after being calcined at 500 °C in air. As seen in Fig. 14, the sodium-free Fe-based AFX catalyst (Fe-AFX_exc) shows good catalytic activity for the SCR of NOx when tested at high reaction temperatures (i.e. above 450 °C), confirming the importance of synthesizing iron-containing zeolites free of alkali cations for this reaction. Interestingly, the catalytic behavior of this Fe-AFX catalyst is comparable to the catalytic activity described in the literature for a well-stablished Fe-CHA catalyst and thus provides an alternative to this framework topology [55].

4. Conclusions

The combination of a bulky rigid organic molecule as OSDA and FAU as the silicon-alumina source has allowed the efficient preparation of high-silica ERI and AFX zeolites with small crystallites of 200 and 30 nm, respectively. These two zeolites have large cavities within their structure with similar length (~13.0 Å), suggesting that the OSDA-2 applied herein presents the adequate shape and size (11.9 × 4.9 Å) to properly fit and stabilize these types of cavities. Copper- and iron-containing ERI and AFX zeolites were synthesized by post-synthetic aqueous exchange or a direct synthesis approach, leading to active catalysts in the NH_3-SCR reaction. However, for producing hydrothermally stable catalysts, alkali cations should be removed. The results presented in this manuscript show the high potential of other metal-containing cage-based zeolites for SCR applications besides the well-established industrial Cu-CHA catalyst. Moreover, they open new opportunities for their use in more structure sensitive catalytic applications, such as for instance redox catalytic applications requiring a fine-tune size control of the encapsulated metal clusters and nanoparticles [13,58].

Acknowledgements

This work has been supported by Haldor Topsøe A/S, by the Spanish Government-MINECO through “Severo Ochoa” (SEV 2012-0267), and MAT2015-71261-R, by the European Union through ERC-AdG-2014-671093 (SynCatMatch) and by the Fundación Ramón Areces through a research contract of the “Life and Materials Science” program. N. M. thanks MINECO for economical support through pre-doctoral fellowship (BES-2013-064347). The authors thank Isabel Millet for technical support.

References

[1] C.S. Cundy, P.A. Cox, The hydrothermal synthesis of zeolites: precursors, intermediates and reaction mechanism, Microporous Mesoporous Mater. 82 (2005) 1–78.
[2] A. Corma, M.E. Davis, Issues in the synthesis of crystalline molecular sieves: towards the crystallization of low framework-Density structures, ChemPhysChem 5 (2004) 304–313.
[3] M.E. Davis, R.F. Lobo, Zeolite and molecular sieve synthesis, Chem. Mater. 4 (1992) 756–768.
[4] R.P. Townsend, Ion exchange in zeolites: some recent developments in theory and practice, Pure Appl. Chem. 58 (1986) 1359–1366.
[5] M. Moliner, C. Martinez, A. Corma, Multipore zeolites: synthesis and catalytic applications, Angew. Chem. Int. Ed. 54 (2015) 3560–3579.
[6] N. Kosinov, J. Gascon, F. Kapteijn, E.J.M. Hensen, Recent developments in zeolite membranes for gas separation, J. Membr. Sci. 499 (2016) 65–79.
[7] E.M. Gallego, et al., Ab initio synthesis of zeolites for preestablished catalytic reactions, Science 355 (2017) 1051–1054.
[8] M. Moliner, C. Martínez, A. Corma, Synthesis strategies for preparing useful small pore zeolites and zeotypes for gas separations and catalysis, Chem. Mater. 26 (2014) 246–258.
[9] S.E. Jee, D.S. Sholl, Carbon dioxide and methane transport in DDR zeolite: insights from molecular simulations into carbon dioxide separations in small pore zeolites, J. Am. Chem. Soc. 131 (2009) 7896–7904.
[10] J.L. White, Methanol-to-hydrocarbon chemistry: the carbon pool (r)evolution, Catal. Sci. Technol. 1 (2011) 1630–1635.
[11] U. Olsbye, et al., Conversion of methanol to hydrocarbons: how zeolite cavity and pore size controls product selectivity, Angew. Chem. Int. Ed. 51 (2012) 5810–5831.
[12] M. Choi, Z. Wu, E. Iglesia, Mercaptosilane-assisted synthesis of metal clusters within zeolites and catalytic consequences of encapsulation, J. Am. Chem. Soc. 132 (2010) 9129–9137.
[13] M. Moliner, et al., Reversible transformation of Pt nanoparticles into single atoms inside high-silica CHA zeolite, J. Am. Chem. Soc. 138 (2016) 15743–15750.
[14] F. Giordanino, et al., Characterization of Cu-exchanged SSZ-13: a comparative FTIR, UV-Vis, and EPR study with Cu-ZSM-5 and Cu-β with similar Si/Al and Cu/Al ratios, Dalton Trans. 42 (2013) 12741–12761.
[15] P. Tian, Y. Wei, M. Ye, Z. Liu, Methanol to olefins (MTO): from fundamentals to commercialization, ACS Catal. 5 (2015) 1922–1938.
[16] N. Martin, et al., Nanocrystalline SSZ-39 zeolite as an efficient catalyst for the methanol-to-olefin (MTO) process, Chem. Commun. 52 (2016) 6072–6075.
[17] J.H. Kwak, R.G. Tonkyn, D.H. Kim, J. Szanyi, C.H.F. Peden, Excellent activity and selectivity of Cu-SSZ-13 in the selective catalytic reduction of NOx with NH3, J. Catal. 275 (2010) 187–190.
[18] A.M. Beale, F. Gao, I. Lezcano-Gonzalez, C.H.F. Peden, J. Szanyi, Recent advances in automotive catalysis for NOx emission control by small-pore microporous materials, Chem. Soc. Rev. 44 (2015) 7371–7405.
[19] R. Martínez-Franco, M. Moliner, P. Concepcion, J.R. Thogersen, A. Corma, Synthesis, characterization and reactivity of high hydrothermally stable Cu-SAPO-34 materials prepared by one-pot processes, J. Catal. 314 (2014) 73–82.
[20] M.J. Wulfers, S. Teketel, B. Ipeka, R.F. Lobo, Conversion of methane to methanol on copper-containing small-pore zeolites and zeotypes, Chem. Commun. 51 (2015) 4447–4450.
[21] F. Gao, et al., Effects of alkali and alkaline earth cocations on the activity and hydrothermal stability of Cu/SSZ-13 NH3–SCR catalysts, ACS Catal. 5 (2015) 6780–6791.
[22] M. Moliner, C. Franch, E. Palomares, M. Grill, A. Corma, Cu-SSZ-39, an active and hydrothermally stable catalyst for the selective catalytic reduction of NOx, Chem. Commun. 48 (2012) 8264–8266.
[23] N. Martin, C.R. Boruntea, M. Moliner, A. Corma, Efficient synthesis of the Cu-SSZ-39 catalyst for DeNOx applications, Chem. Commun. 51 (2015) 11030–11033.
[24] D.W. Fickel, E. D'Addio, J.A. Lauterbach, R.F. Lobo, The ammonia selective catalytic reduction activity of copper-exchanged small-pore zeolites, Appl. Catal. B 102 (2011) 441–448.
[25] A. Rivas-Cardona, J.M. Fedeyko, H.Y. Chen, Molecular Sieve Catalyst for Treating Exhaust Gas, US2016/0096169, 2016.
[26] D.W. Fickel, R.F. Lobo, Copper coordination in cu-SSZ-13 and Cu-SSZ-16 investigated by variable-temperature XRD, J. Phys. Chem. C 114 (2010) 1633–1640.
[27] L.W. Staples, J.A. Gard, The fibrous zeolite erionite; its occurrence, unit cell and structure, Mineral. Mag. 32 (1959) 261–281.
[28] M.K. Rubin, E.J. Rosinski, C.J. Plank, Crystalline Zeolite ZSM-34 and Method of Preparing the Same, US4,086,186, 1978.
[29] I. Bull, U. Muller, Copper Containing ZSM-34, OFF And/or ERI Zeolitic Material for Selective Reduction of NOx, US9,221,015, 2015.
[30] H. Yamada, et al., Downsizing AFX zeolite crystals to nanoscale by a postmilling recrystallization method, Cryst. Growth Des. 16 (2016) 3389–3394.
[31] J.H. Lee, et al., Synthesis and characterization of ERI-type UZM-12 zeolites and their methanol-to-olefin performance, J. Am. Chem. Soc. 132 (2010) 12971–12982.

[32] R.F. Lobo, S.I. Zones, M.E. Davis, Structure-direction in zeolite synthesis, J. Incl. Phenom. Mol. Recognit. Chem. 21 (1995) 47–78.
[33] M. Moliner, F. Rey, A. Corma, Towards the rational design of efficient organic structure-directing agents for zeolite synthesis, Angew. Chem. Int. Ed. 52 (2013) 13880–13889.
[34] M. Moliner, M.J. Díaz-Cabañas, V. Fornés, C. Martínez, A. Corma, Synthesis methodology, stability, acidity, and catalytic behavior of the 18 × 10 member ring pores ITQ-33 zeolite, J. Catal. 254 (2008) 101–109.
[35] Y. Nakagawa, Use of Diels-Alder derived templates to prepare zeolites with multidimensional pore systems, Stud. Surf. Sci. Catal. 84 (1994) 323–330.
[36] Y. Nakagawa, Method for Preparing Crystalline Materials Using Heterobridged Aza-Polycyclic Templating Agents, US5,425,933, 1995.
[37] D. Dorset, S. Weston, S. Dhingra, Crystal structure of zeolite MCM-68: a new three-dimensional framework with large pores, J. Phys. Chem. B 110 (2006) 2045–2050.
[38] A. Cantin, et al., Synthesis and characterization of the all-silica pure polymorph C and an enriched polymorph B intergrowth of zeolite beta, Angew. Chem. Int. Ed. 45 (2006) 8013–8015.
[39] M. Moliner, et al., Synthesis of the Ti-silicate form of BEC polymorph of β-zeolite assisted by molecular modeling, J. Phys. Chem. C 112 (2008) 19547–19554.
[40] S.I. Zones, Y. Nakagawa, Use of modified zeolites as reagents influencing nucleation in zeolite synthesis, Stud. Surf. Sci. Catal. 97 (1995) 45–52.
[41] H. Jon, et al., Effects of structure-directing agents on hydrothermal conversion of FAU type zeolite, Stud. Surf. Sci. Catal. 174A (2008) 229–232.
[42] T. Sonoda, et al., Synthesis of high-silica AEI zeolites with enhanced thermal stability by hydrothermal conversion of FAU zeolites, and their activity in the selectivie catalytic reduction of NOx with NH3, J. Mater. Chem. A 3 (2015) 857–865.
[43] D. Xie, S.I. Zones, C.M. Lew, T.M. Davis, Process Using Molecular Sieve SSZ-98, WO2016/003504, 2016.
[44] N. Martin, M. Moliner, A. Corma, High yield synthesis of high-silica chabazite by combining the role of zeolite precursors and tetraethylammonium: SCR of NOx, Chem. Commun. 51 (2015) 9965–9968.
[45] S. Elomari, S.I. Zones, Method of Making Aluminum-Containing Zeolite with IFR Structure, US2003/0232007, 2003.
[46] T. Moteki, R.F. Lobo, A general method for aluminum incorporation into high-silica zeolites prepared in fluoride media, Chem. Mater. 28 (2016) 638–649.
[47] S. Goel, S.I. Zones, E. Iglesia, Synthesis of zeolites via interzeolite transformations without organic structure-directing agents, Chem. Mater. 27 (2015) 2056–2066.
[48] N. Nakazawa, S. Inagaki, Y. Kubota, Direct hydrothermal synthesis of high-silica SSZ-39 zeolite with small particle size, Chem. Lett. 45 (2016) 919–921.
[49] T. Takata, N. Tsunoji, Y. Takamitsu, M. Sadakane, T. Sano, Nanosized CHA zeolites with high thermal and hydrothermal stability derived from the hydrothermal conversion of FAU zeolite, Microporous Mesoporous Mater. 225 (2016) 524–533.
[50] D. Xie, S.I. Zones, R.J. Saxton, Small Crystal LTL Framework Type Zeolites, WO2016/032565, 2016.
[51] L. Xie, F. Liu, X. Shi, F.S. Xiao, H. He, Effects of post-treatment method and Na co-cation on the hydrothermal stability of Cu–SSZ-13 catalyst for the selective catalytic reduction of NOx with NH3, Appl. Catal. B 179 (2015) 206–212.
[52] I. Bull et al., US Patent 0,226,545, 2008.
[53] S. Brandenberger, O. Kröcher, A. Tissler, R. Althoff, The state of the art in selective catalytic reduction of NOx by ammonia using metal-exchanged zeolite catalysts, Catal. Rev. Sci. Eng. 50 (2008) 492–531.
[54] N. Martin, P.N.R. Vennestrøm, J.R. Thogersen, M. Moliner, A. Corma, Iron-containing SSZ-39 (AEI) zeolite: an active and stable high temperature NH3-SCR catalyst, ChemCatChem 9 (2017) 1754–1757, http://dx.doi.org/10.1002/cctc.201601627.
[55] F. Gao, et al., Iron loading effects in fe/SSZ-13 NH3-SCR catalysts: nature of the Fe ions and structure–function relationships, ACS Catal. 6 (2016) 2939–2954.
[56] J. Perez-Ramirez, et al., Evolution of isomorphously substituted iron zeolites during activation: comparison of Fe-beta and Fe-ZSM-5, J. Catal. 232 (2005) 318–334.
[57] S. Bordiga, et al., Structure and reactivity of framework and extraframework iron in Fe-silicalite as investigated by spectroscopic and physicochemical methods, J. Catal. 158 (1996) 486–581.
[58] L. Liu, et al., Generation of subnanometric platinum with high stability during transformation of a 2D zeolite into 3D, Nat. Mater. 16 (2017) 132–138.